Journal of Magnetic Resonance 307 (2019) 106572

Contents lists available at ScienceDirect

Journal of Magnetic Resonance

journal homepage: www.elsevier.com/locate/jmr

Improved sensitivity of laser-enhanced $^{1}H^{\alpha}$-$^{13}C^{\alpha}$-correlation via suppression of C^{α}-C' scalar-coupling evolution

Hanming Yang, Silvia Cavagnero *

Department of Chemistry, University of Wisconsin – Madison, 1101 University Ave., Madison, WI 53706, USA

ARTICLE INFO

Article history:
Received 11 April 2019
Revised 6 August 2019
Accepted 12 August 2019
Available online 13 August 2019

Keywords:
Hyperpolarization
Photo-CIDNP
LC-photo-CIDNP
NMR sensitivity
$^{1}H^{\alpha}$-$^{13}C^{\alpha}$ correlation

ABSTRACT

Low-concentration photochemically induced dynamic polarization (LC-photo-CIDNP) enables the spectroscopic analysis of biomolecules containing the amino acids Trp and Tyr at sub-micromolar concentration in solution. Typical LC-photo-CIDNP pulse sequences involving ^{1}H-^{13}C correlation, however, perform well in the case of aromatic resonances but display a relatively poor signal-to-noise ratio for $^{13}C^{\alpha}$ and $^{13}C^{\beta}$ resonances. Here, we develop a novel pulse sequence denoted as ^{13}C perturbation-recovered selective-pulse photo-CINDP enhanced reverse INEPT, or ^{13}C PRESPRINT, tailored to the LC-photo-CIDNP analysis of ^{1}H-$^{13}C^{\alpha}$ pairs. Our method, which is based on full suppression of 1-bond C^{α}-C' scalar-coupling evolution during the constant-time delay, results into a sensitivity improvement by a factor of 2. The enhanced performance of this pulse sequence enabled us to improve the analysis of LC-photo-CIDNP laser-power dependence at very low (200 nM) sample concentration. An improved theoretical model, developed to quantitatively describe this laser-power dependence, shows excellent agreement with our ^{13}C PRESPRINT experimental data.

1. Introduction

Photochemically induced dynamic nuclear polarization (photo-CIDNP) is an established magnetic-resonance technique [1–6] that has been recently exploited in liquid-state NMR to enhance the sensitivity of biomolecules carrying aromatic functional groups [7–18]. A main advantage of photo-CIDNP is the fast (~0.2 s) *in situ* generation of nuclear hyperpolarization under physiologically relevant conditions.

Low-concentration photo-CIDNP [10] (LC-photo-CIDNP) is a branch of this method that requires specific photo-sensitizers that are tailored to sub-μM sample concentrations and oxygen-scavenging agents. LC-photo-CIDNP is typically performed in the presence of cryogenic probes, and it enables the rapid detection of tryptophan (Trp) and tyrosine (Tyr), either in their free state or within proteins, down to 200–500 nM concentration.

C^{α} and, to a lesser extent, H^{α} chemical shifts yield semi-quantitative information on protein secondary structure [19]. Hence, detecting C^{α}-H^{α} pairs at the highest possible sensitivity is particularly desirable. ^{13}C PREPRINT (Fig. 1B) is a LC-photo-CIDNP pulse sequence tailored to the ultra-sensitive detection of aromatic H-C or H^{α}-C^{α} pairs in Trp (Fig. 1A) and Tyr, in isolation or within proteins [10]. This pulse sequence is particularly useful for the characterization of backbone secondary structure of proteins via H^{α}-C^{α} pairs.

^{13}C PREPRINT includes a constant-time period T, which is typically optimized for evolution of the one-bond C^{α}-C^{β} scalar coupling interaction ($^{1}J_{C^{\alpha}C^{\beta}}$=33.5 Hz, Fig. 1A). On the other hand, $^{13}C^{\alpha}$s are also coupled to $^{13}C'$ with a $^{1}J_{C^{\alpha}C'}$ close to 53.4 Hz (Fig. 1A). Hence, evolution of the one-bond C^{α}-carbonyl carbon (i.e., C^{α}-C') scalar coupling interaction during T leads to additional terms in the Hamiltonian, resulting in $^{13}C^{\alpha}$ coherence loss. The situation is further complicated by Bloch-Siegert effects [20] experienced by $^{13}C'$, given that the ^{13}C carrier frequency is centered on $^{13}C^{\alpha}$, in experiments aimed at detecting H^{α}-C^{α} pairs. In summary, significant signal losses occur as the result of both of the above effects.

Here, we present a modified version of the ^{13}C PREPRINT pulse sequence, denoted as ^{13}C PRESPRINT (perturbation-recovered selective-pulse photo-CIDNP enhanced reverse INEPT), that circumvents the above disadvantages. LC-photo-CIDNP signal-to-noise (S/N) is known to depend weakly on laser irradiation power [10]. The enhanced sensitivity achieved via ^{13}C PRESPRINT enabled us to quantitatively analyze the power dependence of LC-photo-CIDNP at very low sample concentration (200 nM) across a wider range of laser powers than previously possible, starting at 50 mW. In addition, we developed an improved theoretical model to predict the LC-photo-CIDNP laser-power dependence. This

* Corresponding author.
E-mail address: cavagnero@chem.wisc.edu (S. Cavagnero).

https://doi.org/10.1016/j.jmr.2019.106572
1090-7807/

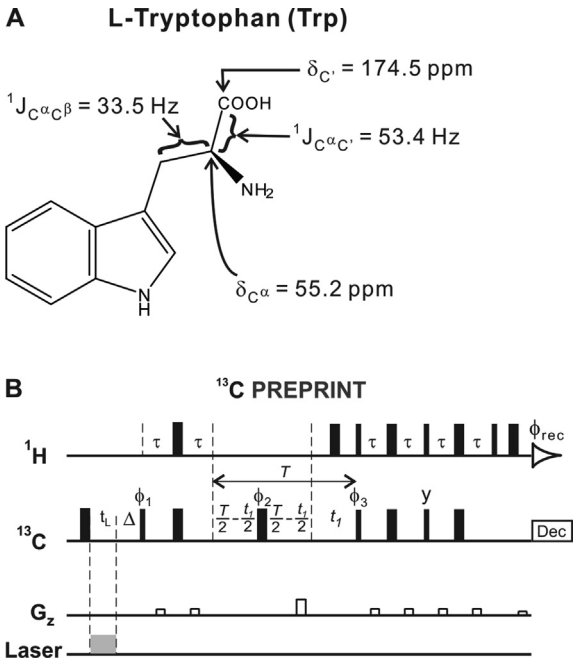

Fig. 1. (A) Structure of L-tryptophan (Trp), highlighting relevant chemical shifts and scalar coupling constants. Numerical values of chemical shifts and coupling-constants were determined experimentally in 90% H_2O and 10% D_2O at room temperature via a simple 1D pulse-acquire ^{13}C sequence. (B) scheme illustrating the ^{13}C PREPRINT pulse sequence [10].

model was shown to adequately fit experiment data, and was therefore able to account for a wider laser-power range than previously possible.

2. Results and discussion

2.1. Suppression of $C^\alpha C'$ scalar-coupling evolution leads to improved sensitivity in LC-photo-CIDNP ^{1}H-^{13}C correlation

In the conventional ^{1}H-^{13}C heteronuclear-correlation ^{13}C PREPRINT pulse sequence [10] (Fig. 1B) optimized for the detection of C^α resonances, some of the $^{13}C^\alpha$ coherence is lost due to two independent effects.

First, the widely different values of the $^1J_{C^\alpha C'}$ (53.4 Hz) and $^1J_{C^\alpha C^\beta}$ (33.5 Hz) scalar-coupling constants prevent the C^α-C' scalar-coupling interaction from evolving by exactly 180° during the constant time T. The duration of T is typically optimized for 180° evolution of the C^α-C^β scalar-coupling interaction ($T \sim 1/\ ^1J_{C^\alpha C^\beta} - 2\tau$, empirically optimized to 26.6 ms). Note that the scalar-coupling constants reported here are for the ^{13}C-^{15}N-labeled photo-CIDNP-active amino acid Trp. As a result, T is not optimized for C^α-C' coupling, resulting in significant signal losses. For illustrative purposes, the above can be readily verified (upon ignoring off-resonance effects and pulse-field gradients) by considering the experimentally detectable product operators at the end of the constant time: $2\hat{I}_z\hat{A}_x\cos[\pi^1J_{C^\alpha C'}(2\tau+T)]\ \cos[\pi^1J_{C^\alpha C^\beta}(2\tau+T)]\cos(\omega_A t_1)+2\hat{I}_z\hat{A}_y\cos[\pi^1J_{C^\alpha C'}(2\tau+T)]\cos[\pi^1J_{C^\alpha C^\beta}(2\tau+T)]\sin(\omega_A t_1)$, where the symbols $\hat{I}_z$ and $\hat{A}_{x,y}$ refer to the pertinent components of the nuclear-spin angular-momentum operators of H^α and C^α, respectively, ω_A is the angular precession frequency of the C^α spin in the rotating frame, and the time delays τ and T are defined as in Fig. 1B.

Second, the widely different chemical shifts of the Trp C' (174.5 ppm) and C^α (55.2 ppm) generate Bloch-Siegert effects (ca. 119 ppm off-resonance from the carrier frequency) on the carbonyl carbon, given that the ^{13}C pulses are centered in the C^α spectral region.

To quantify the extent of the above complications, we carried out computer simulations estimating relative expected signals in ^{13}C PREPRINT experiments in the absence and presence of C^α-C' scalar coupling and off-resonance effects. The results are shown in Fig. 2A (see also Supporting Information for details). Interestingly, the simulated ^{13}C PREPRINT signal is expected to increase slightly as the ^{13}C π hard-pulse duration gets longer. This result applies to both dark (i.e., laser off) and light (i.e., laser on) conditions. The duration of this pulse is ca. 24 μs ($\gamma B_1 = 20.83$ kHz) for our NMR probe, i.e., a typical value on modern NMR spectrometers.

As apparent in Fig. 2A and more explicitly highlighted in Fig. 2B, the predicted signal increases by ca. 2-fold when C^α-C' scalar-coupling evolution and off-resonance effects are not present.

Encouraged by the above predictions, we proceeded to implement the following updates to the ^{13}C PREPRINT pulse sequence. First, we replaced a few key ^{13}C hard π pulses with corresponding semi-selective pulses (not exciting the carbonyl carbons) centered in the C^α region, to refocus the C^α-C' scalar-couplings. Semi-selective excitation was carried out with the Q3_surbop pulse, which is an improved version the Q3 pulse shape [21]. This pulse

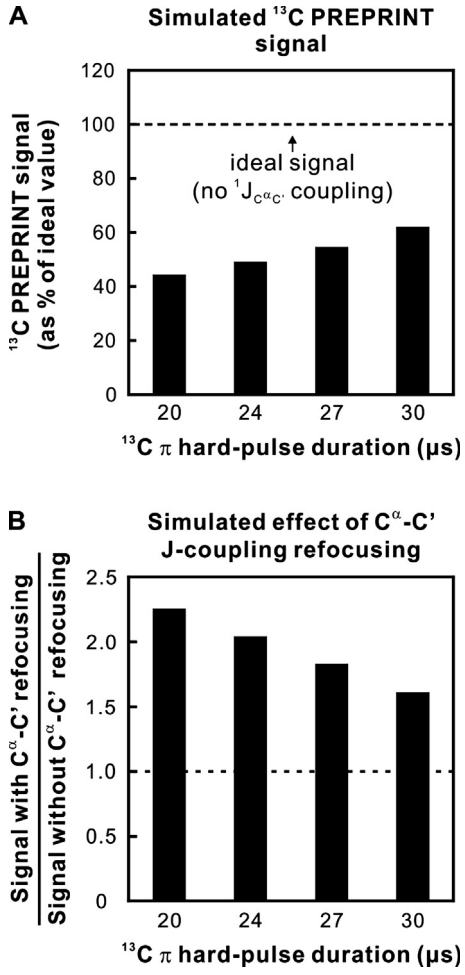

Fig. 2. (A) Simulated ^{13}C PREPRINT signal of Trp H^α as a function of ^{13}C π hard-pulse duration, assuming a 600 MHz NMR spectrometer. (B) Simulated ratio of ^{13}C PREPRINT S/N of Trp H^α as a function of ^{13}C π hard-pulse duration, for a 600 MHz NMR spectrometer.

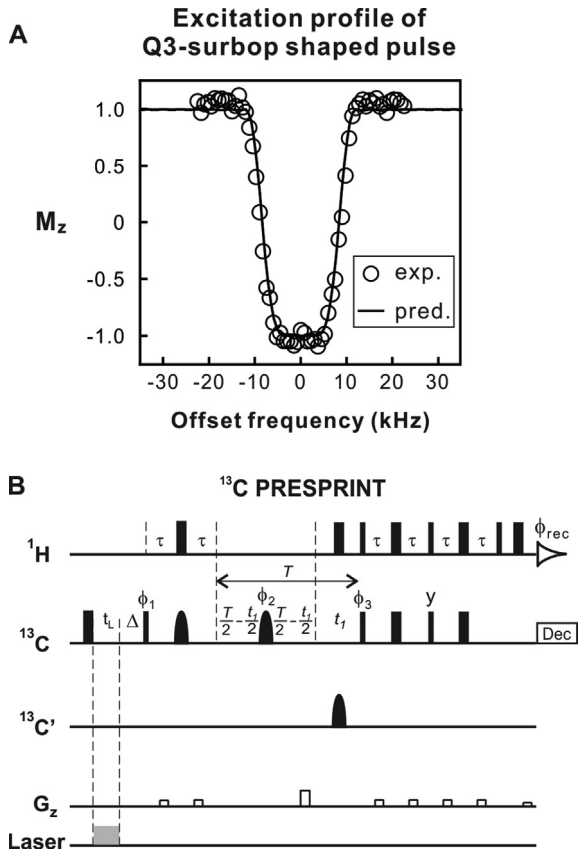

Fig. 3. (A) Excitation profile of 180° ^{13}C Q3_surbop shaped pulse used in the ^{13}C PRESPRINT pulse sequence. The predicted excitation profile was generated via the Bruker waveform simulator. Experimental data points were generated upon changing the center frequency of the 180° ^{13}C shaped pulse of a simple reference pulse sequence (see Supporting Fig. S2). (B) ^{13}C PRESPRINT pulse sequence. The inverted-bell shapes denote Q3_surbop shaped pulses (180° flip angle), which are improved versions of the Q3 selective pulse [21] developed by Bruker. The symbol t_L denotes laser irradiation time, Δ is the perturbation-recovery delay, $\tau = 1/(4\,J_{CH})$, and T is the total evolution time in the indirect dimension (optimized to 26.6 ms for C^{α}). The phase cycling is $\phi_{rec} = x, -x, -x, x$; $\phi_1 = y, -y$; $\phi_2 = y, y, -x, -x, -y, -y, x, x$. For convenience, a direct side-by-side comparison between the ^{13}C PRESPRINT and ^{13}C PREPRINT pulse sequences is provided in Supporting Fig. S3.

has an excellent excitation profile, as shown in Fig. 3A. When centered in the $^{13}C^{\alpha}$ region, Q3_surbop produced negligible excitation in the ^{13}C' region, which is ca. 18 kHz off-resonance from the pulse center frequency, at 600 MHz. An additional Q3_surbop band-selective ^{13}C pulse centered on the ^{13}C' resonances was introduced during t_1 evolution, to decouple ^{13}C'from $^{13}C^{\alpha}$, thus preventing any peak splitting in the indirect dimension due to $^{1}J_{C^{\alpha}C'}$ coupling (see 2D spectrum in Supporting Fig. S4).

We denote the resulting improved pulse sequence, shown in Fig. 3B, as ^{13}C-perturbation-recovered band-selective-photo-CIDNP enhanced reverse INEPT, or ^{13}C PRESPRINT (note the relatively minor spelling difference relative to ^{13}C PREPRINT). Conveniently, this pulse sequence achieves complete refocusing of C^{α}-C' scalar coupling, and off-resonance effects are no longer present. The performance of ^{13}C PRESPRINT was experimentally tested and compared with that of ^{13}C PREPRINT.

Data were first collected on 2 μM uniformly ^{13}C-^{15}N-labeled Trp (32 scans, ~1 min. total experiment time). As shown in Fig. 4A, under light (laser on) conditions a fairly high S/N was rapidly observed for ^{13}C PRESPRINT. This value is ca. 2-fold higher than the S/N achieved for ^{13}C PREPRINT, in full agreement with the computer simulations. At 200 nM Trp (Fig. 4B), a similar 2-fold gain was achieved, though the S/N was lower, due to both the lower

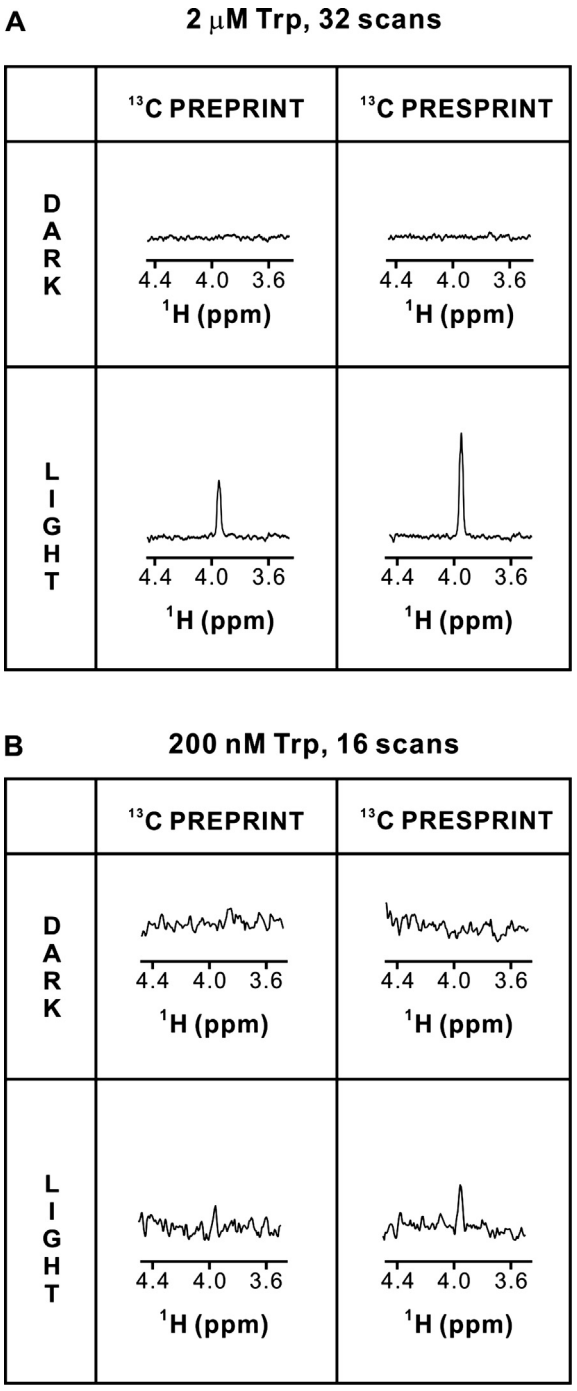

Fig. 4. Comparison between 1D ^{13}C PREPRINT and ^{13}C PRESPRINT spectra of (A) 2 μM and (B) 200 nM ^{13}C-^{15}N-enriched Trp in 90% H_2O and 10% D_2O. Data for each dark/light experiment pair were collected on identical independently prepared samples, with the same experimental parameters and conditions except for pulse-sequence-dependent values. Spectra were acquired with 2630 total points and a sweep width of 6602 Hz. The recycle delay was 2.5 s. Spectra were zero-filled to 4096 complex points, and an exponential window function was applied (5 Hz line-broadening). ^{13}C PRESPRINT shows a 2-fold higher S/N than ^{13}C PREPRINT, under light conditions.

concentration and the smaller number of acquired transients. When we measured the experimental enhancement on a different cryogenic probe with a longer ^{13}C π pulse (i.e., 30 instead of 24 μs, data not shown), the results were consistent with the theoretical predictions of Fig. 2.

The ^{13}C PRESPRINT pulse sequence was also tested on free tyrosine (Tyr) in solution (Supporting Fig. S5). However, due to the

much lower photo-CIDNP polarization of Tyr C^{α}, enhancement values could not be quantified.

2.2. Theoretical prediction of laser-power dependence of LC-photo-CIDNP at nanomolar sample concentration

LC-photo-CIDNP enhancements depend strongly on laser irradiation power at high sample concentration, i.e., ≥μM. On the other hand, this dependence is known to be significantly weaker at lower sample concentrations, i.e., ≤500 nM [10]. Recent investigations by Cavagnero and coworkers showed that steady-state photo-CIDNP polarization at low sample concentration (typically < 1 μM), where the free-radical of the molecule of interest $M^{\bullet+}$ undergoes complete nuclear spin relaxation before termination, can be quantitively described by a theoretical expression [10]. This sample-concentration regime typically obeys the condition $1/T_1^{M^{\bullet+}} >> k_{ter}[M^{\bullet+,SS}] + k_{de}[M^{SS}]$, where $T_1^{M^{\bullet+}}$ is the spin-lattice nuclear relaxation time of the molecule of interest in free-radical form, k_{ter} is the effective rate constant for the regeneration of M taking into account all the elementary steps leading to it starting from $M^{\bullet+}$ [18,22], k_{de} is the rate constant for degenerate electron exchange, and the symbols $[M^{SS}]$ and $[M^{\bullet+,SS}]$ denote the steady-state concentrations of the molecule of interest in neutral and free-radical form. Under the above conditions, the steady-state polarization of the k^{th} nucleus, P_k^{SS}, is [10]

$$P_k^{M,SS} = \frac{T_1^M k_{et}\left[{}^TD^{SS}\right][M^{SS}](1+\gamma)\xi^G\Phi_G}{[M]_o} \quad (1)$$

where γ is defined as

$$\gamma = \left(\frac{\xi^F(1-\Phi_G)}{\xi^G\Phi_G}\right) \quad (2)$$

with ξ_k^F and ξ_k^G denoting the normalized probability differences to generate a recombination product in the α and β spin states of the k^{th} nucleus per F-pair and geminate recombination event, respectively. The parameter Φ_G denotes the total probability of geminate recombination per geminate radical pair. The initial concentrations of the molecule of interest are $[M]_0$. The symbols $\left[{}^TD^{SS}\right]$ and $[D^{\bullet-SS}]$ denote steady-state concentrations of the dye in the triplet excited-state and radical forms, respectively. The effective rate constant for the bimolecular electron transfer between the molecule of interest M and the triplet excited-state dye ${}^TD$ is denoted as k_{et}. Finally, T_1^M is the spin-lattice nuclear relaxation times of the k^{th} nucleus in M.

Under steady-state conditions and nanomolar sample concentration, it can be shown (see Supporting Information for details) that

$$[M^{SS}] \approx \frac{(k_{ter}/k_{et})([M]_o)^2}{\left[{}^TD^{SS}\right]} - 2\frac{(k_{ter}/k_{et})^2([M]_o)^3}{\left[{}^TD^{SS}\right]^2} \quad (3)$$

Upon substitution of relation (3) into (1), the steady-state polarization can be expressed as

$$P_k^{M,SS} \approx T_1^M k_{ter}(1+\gamma)\xi^G\Phi_G[M]_0\left(1 - 2\frac{[M]_0(k_{ter}/k_{et})}{\left[{}^TD^{SS}\right]}\right) \quad (4)$$

Given Eq. (4) and the fact that $\left[{}^TD^{SS}\right]$ is directly proportional to laser irradiation power P_{light} (see Supporting Information), and given that the signal S under light conditions is directly proportional to the extent of steady-state polarization [23], the laser power dependence of LC-photo-CIDNP can be expressed as

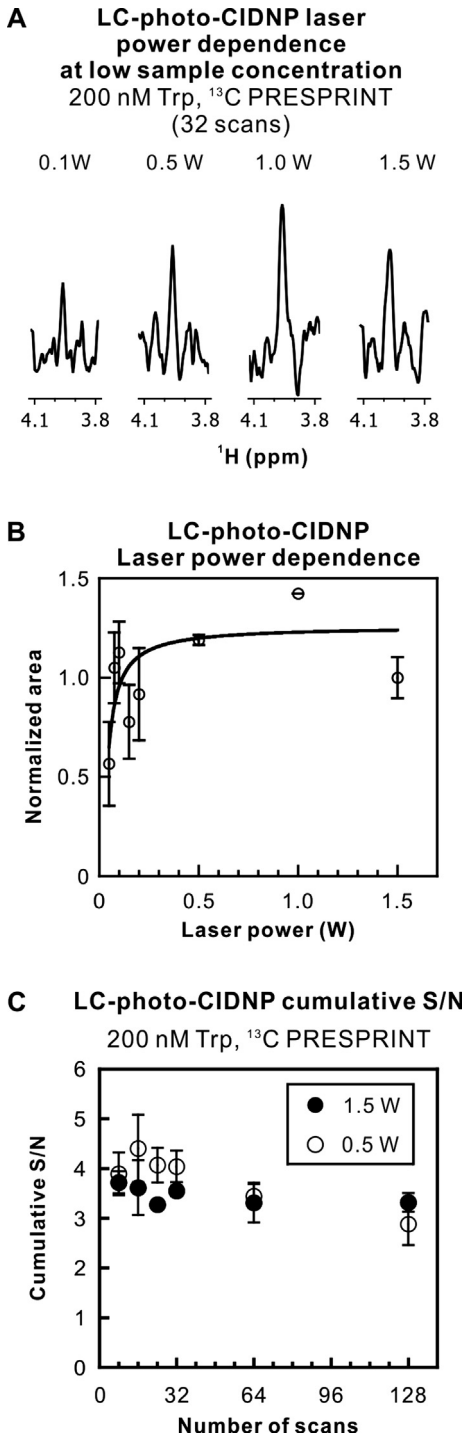

Fig. 5. (A) Representative 1D ^{13}C PRESPRINT light spectra illustrating the LC-photo-CIDNP laser-power dependence of 200 nM ^{13}C-^{15}N Trp. (B) Plot illustrating the ^{13}C PRESPRINT (light conditions) H^{α}-resonance area as a function of laser irradiation power. Areas were normalized relative to the average area at 1.5 W laser power. The solid line denotes the curve fit based on the theoretical model developed in this work (Eq. (5), with a and b regarded as adjustable parameters). (C) Cumulative ^{13}C PRESPRINT S/N as a function of number of scans at 0.5 and 1.5 W laser power. A total of 2402 points, a 6010 Hz sweepwidth and a 2.5 s recycle delay were used in each experiment. Spectra were zero-filled to 4096 complex points, and an exponential window function was applied (10 Hz line-broadening). Data in panels B and C are reported as average ± S.E. for n = 3.

$$S = a - b \cdot P_{light}^{-1} \quad (5)$$

where a and b are adjustable parameters.

2.3. Laser power dependence of LC-photo-CIDNP at nanomolar Trp concentration

We previously found that LC-photo-CIDNP enhancements depend more steeply on laser-irradiation power at > μM sample concentration than at lower concentration. [10] Although we were previously able to detect 200 nM Trp via LC-photo-CIDNP, the poor S/N prevented us from quantitatively investigating the laser power dependence of LC-photo-CIDNP within the low-concentration regime ($\leq$ 500 nM) at very low laser power (ca. 50 mW). This dependence is important to experimentally validate photo-CIDNP theoretical models at low laser power and sample concentration.

The improved sensitivity of ^{13}C PRESPRINT over ^{13}C PREPRINT is of general significance. Next, we provide a specific example of a useful application. Fig. 5A shows how the improved ^{13}C PRESPRINT sensitivity enables investigating the LC-photo-CIDNP laser-power dependence. Data at very low sample concentration (i.e. 200 nM Trp) were collected over a wide range of laser powers, starting at 0.05 W. As illustrated in Fig. 5B, the experimental laser-power dependence shows good agreement with the theoretical model developed here, based on Eq. (5).

Finally, we compared the cumulative S/N as a function of number of transients, at 0.5 and 1.5 W, to probe whether the extent of photodegradation varies at widely different laser power levels (Fig. 5C) and at very low sample concentration (200 nM). We did not find significant differences between the two power settings. We conclude that collecting LC-photo-CIDNP data at low laser power at nM sample concentration does not lead to any increases in the extent of photodegradation. In summary, the data in Fig. 5 are important because they highlight that LC-photo-CIDNP can be performed with the ^{13}C PRESPRINT pulse sequence at low laser power (> 0.2 W), and yields excellent NMR sensitivity with no photodegradation penalties relative to higher-laser-power conditions.

3. Conclusions

A ca. 100 % improvement in S/N over ^{13}C PREPRINT has been achieved with our newly-developed ^{13}C PRESPRINT pulse sequence. This experimental advance enabled us to quantitatively assess the weak power dependence of photo-CIDNP at low sample concentration. The theoretical model that we developed to describe this laser-power dependence is fully consistent with our experimental data. In summary this study highlights the exciting prospect to perform LC-photo-CIDNP at nM concentration with the ^{13}C PRESPRINT pulse sequence employing low-power inexpensive and readily available light sources.

4. Experimental methods

4.1. Materials

^{13}C-^{15}N-Trp and the fluorescein photosensitizer dye were purchased from Cambridge Isotopes (Tewksbury, MA) and Sigma-Aldrich (St. Louis, MO), respectively. The oxygen-scavenging enzymes glucose oxidase (GO, from *Aspergillus niger*, catalog number G7141, EC 1.1.3.4) and catalase (CAT, from bovine liver, catalog number C40, EC 1.11.1.6) were purchased from Sigma-Aldrich (St. Louis, MO). Enzymes were dissolved in 10 mM potassium phosphate (pH 7.0), divided into single-use aliquots, flash-frozen in liquid nitrogen and stored at −80 °C.

4.2. NMR sample preparation

All NMR samples contained 10 % D_2O, 10 mM potassium phosphate buffer (pH 7.2), 0.15 μM GO, 0.10 μM CAT, and 2.5 μM fluorescein. In addition, D-glucose (2.5 mM) was added to the NMR samples c.a. 10 min. prior to data collection.

4.3. Photo-CIDNP NMR experiments

All photo-CIDNP experiments were carried out with a continuous-wave (CW) argon-ion laser (INNOVA SABRE DBW 24/7 Coherent Inc., Santa Clara, CA) operating in single-line mode (488 nm). The laser beam was directed inside the NMR spectrometer via a convex lens (LB4330, Thorlabs, Newton, NJ), a fiber-coupler (F-91-C1-T, Newport Corporation) and a fused silica optical fiber with 0.6 mm core diameter (FDP600660710, Molex, Lisie, IL). The optical fiber was guided into a glass coaxial insert (WGS-5BL, Wilmad-Labglass, Buena, NJ), which was inserted into the NMR tube to ensure that laser beam was centered within the NMR tube. Laser power was assessed at the tip of the coaxial insert via a power meter.

All NMR spectra were collected at 25 °C with an Avance III HD 600 MHz spectrometer (Bruker Biospin Corp., Billerica, MA). A ^{1}H {^{19}F/^{13}C/^{15}N} triple-resonance (TCI) cryogenic probe fitted with a z-gradient was used for all experiments unless otherwise stated (12 μs ^{13}C π/2 pulse duration). In some experiments (see Section 2.1), a ^{1}H{^{13}C/^{15}N} triple-resonance (TXI) cryogenic probe (15 μs ^{13}C π/2 pulse duration) fitted with a z gradient was employed to measure ^{13}C PRESPRINT enhancements for a different ^{13}C π hard-pulse duration. This TXI probe had the transmitter/receiver coils and the ^{1}H and ^{2}H preamplifiers (but not the ^{13}C and ^{15}N pre-amplifiers) cooled to cryogenic temperature. This probe displayed similar sensitivity to the TCI probe for ^{1}H-detected experiments carried out in this work.

The carrier frequency was centered on the solvent resonance (4.70 ppm) in the ^{1}H channel, and at 55 ppm (C^{α} region) in the ^{13}C channel. All spectra were referenced with external 4,4-dimethyl-4-silapentane-1-sulfonic acid (DSS). Data were processed with the MestRe Nova (version 11.0.1-20560, Mestrelab Research, Spain). Spectral widths, total number of points and window functions are as listed in individual figure legends.

4.4. Computer simulations

Computer simulations in Fig. 2 were carried out with Mathematica (version 11.2.0.0, Wolfram Research, Champaign, IL) using procedures described in the Supporting Information. The simulation input included definitions of spin operators, scalar couplings, chemical shifts, pulse strengths, as well as rotation and density matrices. The output of the simulations (see Fig. 2A) were numerical values proportional to the expected NMR signal, defined as in equation S4 of the Supporting Information.

Acknowledgments

We are grateful to Miranda F. Mecha for a critical reading on the manuscript, and to Lingchao Zhu, Charlie Fry and Heike Hofstetter for technical assistance. We also thank Charlie Fry and Clemens Anklin for helpful discussions. We acknowledge funding from the National Institutes of Health (Grants R01GM125995, S10RR13866-01 and S10OD012245).

Appendix A. Supplementary material

Supplementary data to this article can be found online at https://doi.org/10.1016/j.jmr.2019.106572.

References

[1] P.J. Hore, A. Volbeda, K. Dijkstra, R. Kaptein, Photoreduction of flaving by NADH. A flash photolysis photo-CIDNP study, J. Am. Chem. Soc. 104 (1982) 6262–6267.

[2] H.R. Ward, R.G. Lawler, Nuclear magnetic resonance emission and enhanced absorption in rapid organometallic reactions, J. Am. Chem. Soc. 89 (1967) 5518–5519.

[3] J. Bargon, H. Fischer, U. Johnsen, Nuclear magnetic resonance emission lines during fast radical reactions. I. Recording Methods and Examples, Z. Naturforsch. A 22 (1967) 1551–1555.

[4] M. Goez, Photo-CIDNP spectroscopy, Annu. Rep. NMR Spectrosc. 66 (2009) 77–147.

[5] P.J. Hore, R.W. Broadhurst, Photo-CIDNP of biopolymers, Prog. Nucl. Magn. Reson. Spectrosc. 25 (1993) 345–402.

[6] L.T. Kuhn, Photo-CIDNP NMR spectroscopy of amino acids and proteins, Hyperpolar. Meth. NMR Spectrosc. 338 (2013) 229–300.

[7] A. Sekhar, S. Cavagnero, EPIC- and CHANCE-HSQC: two ^{15}N-photo-CIDNP-enhanced pulse sequences for the sensitive detection of solvent-exposed tryptophan, J. Magn. Reson. 200 (2009) 207–213.

[8] A. Sekhar, S. Cavagnero, ^{1}H photo-CIDNP enhancements in heteronuclear correlation NMR spectroscopy, J. Phys. Chem. B 113 (2009) 8310–8318.

[9] Y. Okuno, S. Cavagnero, Fluorescein: a photo-CIDNP sensitizer enabling hypersensitive NMR data collection in liquids at low micromolar concentration, J. Phys. Chem. B 120 (2016) 715–723.

[10] Y. Okuno, M.F. Mecha, H. Yang, L. Zhu, C.G. Fry, S. Cavagnero, Laser- and cryogenic-probe-assisted NMR enables hypersensitive analysis of biomolecules at sub-micromolar concentration, Proc. Natl. Acad. Sci. 116 (2019) 11602–11611.

[11] C.E. Lyon, J.A. Jones, C. Redfield, C.M. Dobson, P.J. Hore, Two-dimensional ^{15}N–^{1}H photo-CIDNP as a surface probe of native and partially structured proteins, J. Am. Chem. Soc. 121 (1999) 6505–6506.

[12] J.H. Lee, A. Sekhar, S. Cavagnero, ^{1}H-detected ^{13}C photo-CIDNP as a sensitivity enhancement tool in solution NMR, J. Am. Chem. Soc. 133 (2011) 8062–8065.

[13] J.H. Lee, S. Cavagnero, A novel tri-enzyme system in combination with laser-driven NMR enables efficient nuclear polarization of biomolecules in solution, J. Phys. Chem. B 117 (2013) 6069–6081.

[14] R. Kaptein, K. Dijkstra, K. Nicolay, Laser photo-CIDNP as a surface probe for proteins in solution, Nature 274 (1978) 293–294.

[15] M. Mompean, R.M. Sanchez-Donoso, A. de la Hoz, V. Saggiomo, A.H. Velders, M. V. Gomez, Pushing nuclear magnetic resonance sensitivity limits with microfluidics and photo-chemically induced dynamic nuclear polarization, Nat. Commun. 9 (2018) 108.

[16] K.L. Ivanov, A.N. Pravdivtsev, A.V. Yurkovskaya, H.M. Vieth, R. Kaptein, The role of level anti-crossings in nuclear spin hyperpolarization, Prog. Nucl. Magn. Reson. Spectrosc. 81 (2014) 1–36.

[17] K.L. Ivanov, A. Wagenpfahl, C. Deibel, J. Matysik, Spin-chemistry concepts for spintronics scientists, Beilstein J. Nanotechnol. 8 (2017) 1427–1445.

[18] Y. Okuno, S. Cavagnero, Effect of heavy atoms on photochemically induced dynamic nuclear polarization in liquids, J. Magn. Reson. 286 (2018) 172–187.

[19] S. Spera, A. Bax, Empirical correlation between protein backbone conformation and C^{α}. and C^{β}. ^{1}3C nuclear magnetic resonance chemical shifts, J. Am. Chem. Soc. 113 (1991) 5490–5492.

[20] R. Freeman, A Handbook of Nuclear Magnetic Resonance, Wiley, New York, 1988.

[21] L. Emsley, G. Bodenhausen, Optimization of shaped selective pulses for NMR using a quaternion description of their overall propagators, J. Magn. Reson. 97 (1992) 135–148.

[22] Y. Okuno, S. Cavagnero, Photochemically induced dynamic nuclear polarization: basic principles and applications, eMagRes 6 (2017) 283–313.

[23] J.H. Lee, Y. Okuno, S. Cavagnero, Sensitivity enhancement in solution NMR: emerging ideas and new frontiers, J. Magn. Reson. 241 (2014) 18–31.